Acoustic characterization of a vessel-mounted turbine during the Agate Pass deployment

1 Introduction

Aquatic animals depend on sound for a wide range of activities, including communication, navigation, and foraging. Anthropogenic noise can impact their ability to perform these life-sustaining actions, lead them to alter their behavior, or, in extreme cases, even damage hearing or cause barotrauma (Polagye and Bassett 2020). While marine renewable energy has the potential to reduce negative impacts on the environment by reducing contributions to climate change, it is imperative to consider the full range of possible environmental effects. Therefore, we must be able to accurately measure and predict sound produced by marine energy converters to ensure that noise levels fall within regulatory limits, minimizing harm to marine animals.

Though studies to date suggest that sound produced by prototype tidal turbines are unlikely to impact aquatic animals (Polagye and Bassett 2020), identifying turbine noise *in situ* remains a major challenge. Specifically, relatively low levels of radiated sound from turbines can be difficult to distinguish from ambient noise. In addition, the various moving parts of the turbine—the power electronics, servomotor, and driveline—all have the potential to produce sound. The characteristics of these noises are not well established, making it difficult to predict overall radiated noise.

Our approach employs several measures to differentiate between turbine and ambient noise. First, we use drifting acoustic instruments to collect the data, minimizing flow noise. Second, before measuring the turbine operating in a tidal channel, we collected acoustic data at close range (< 2 m) while it was being motored dockside. This process identifies specific frequency ranges where turbine signals are most likely to present, making them easier to find in environments with a lower signal-to-noise ratio. Third, we use localization to attribute the source of acoustic signals. Though we could not identify any localizable signals from the turbine due to low signal-to-noise ratios, we do localize several other sounds that demonstrate the effectiveness of the methodology and its applicability to future turbine measurements.

2 Methods

2.1 Turbine and Deployment Site

Agate Pass is a tidal channel separating the north end of Bainbridge Island and the Kitsap Peninsula in Puget Sound, Washington. Mixed semidiurnal tides in the region drive strong tidal exchange through this relatively narrow (~250 m) and shallow (~6 m) passage connecting the main basin of Puget Sound to the waters surrounding western Kitsap County. Tidally driven currents in Agate Pass can reach 2.5 m/s during strong spring tides but only reached 2 m/s during our survey. Agate Pass was selected for testing a tidal turbine mounted to a moored vessel due the combination of strong currents and proximity to the University of Washington in Seattle.

Relatively high volumes of vessel traffic and the narrow width of Agate Pass dictated that the turbine be positioned outside of the most constricted areas with highest currents (Harrison et. al. 2023). Consequently, R/V Russel David Light (RDL), the vessel on which the tidal turbine was mounted, was moored in 8 m of water at the southern end of Agate Pass at 47.7070° N, 122.5705° W (Figure 1) from 18-23 April 2022. This location offered a combination of moderate currents, shallow water, favorable sandy substrate for anchors, and relative protection from the metocean conditions of Puget Sound's main basin.

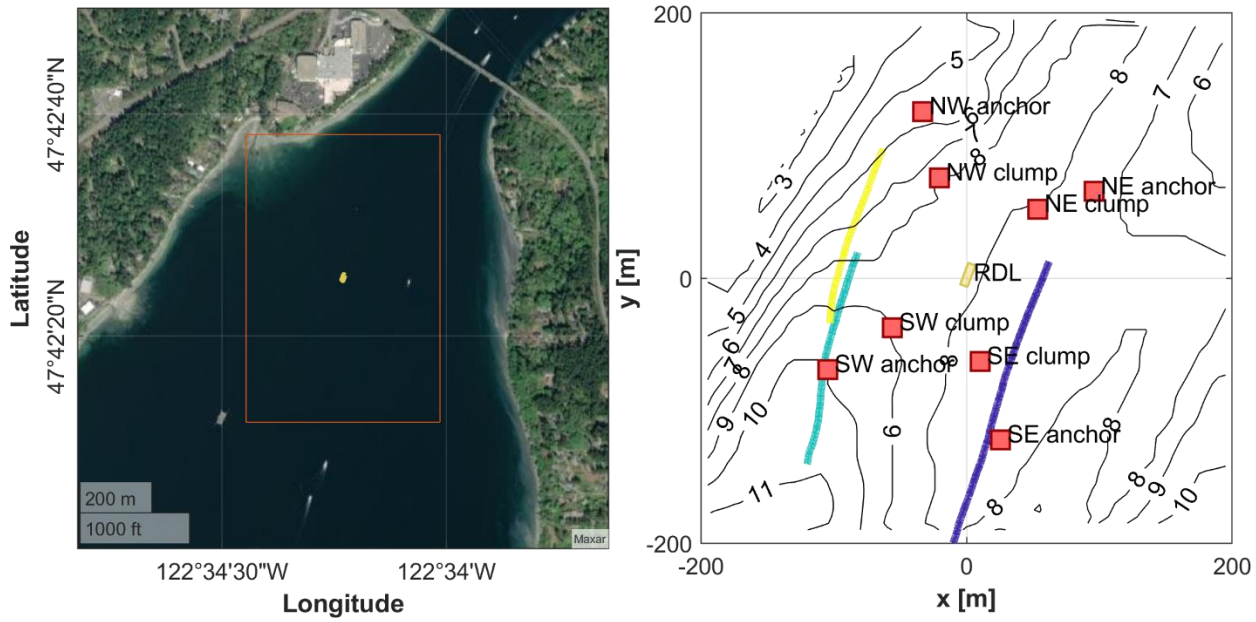

Figure 1: Agate Pass deployment site. (left) Satellite imagery of the southern portion of Agate Pass with RDL's location marked at the center of the box. (right) Overview of site bathymetry, components of the anchor system, location of RDL throughout the deployment, and three representative DAISY tracks.

Acoustic measurements were collected during a relatively strong flood tide on 20 April 2022 between 15:58-17:42 local time. During data collection, there was persistent light rain. Wind-driven waves were small (less than 15 cm), with little to no white capping. A few vessels passed by the deployment site, and measurements were paused while they were within approximately 2 km to minimize their presence in recordings. Vehicle traffic on the Agate Pass Bridge, located approximately 700 meters north of RDL, may have also contributed to the soundscape.

The turbine being characterized was deployed from a gantry aboard RDL, a 20-m long aluminum-hulled catamaran purpose-built for turbine testing. The gantry is located between the hulls near the bow of the vessel, forward of the lab spaces and wheelhouse. During testing, the rotor and generator housing were submerged such that the top of the generator housing and rotor were approximately 0.2 m and 1 m below the surface, respectively. For the duration of measurements, a 30 kW Northern Lights M30C3F generator (1800 rpm) was in operation to provide electrical power for RDL.

RDL was anchored in a four-point moor (Figure 1) with the bow facing roughly NNW into the flood currents. Each leg of the mooring included a 681 kg Danforth anchor with a large surface float. In-line between the anchor and RDL was 59 m of wire rope and chain terminating at a 1055 kg cast-iron clump weight (Figure 2). To support deployment and recovery operations, Viny 12B-3 floats were attached to chains near the anchors and clump weights. As discussed in Section 3.3.2, vibrations of the various floats, lines, shackles, and other supporting hardware, particularly the clump weights, produced noise.

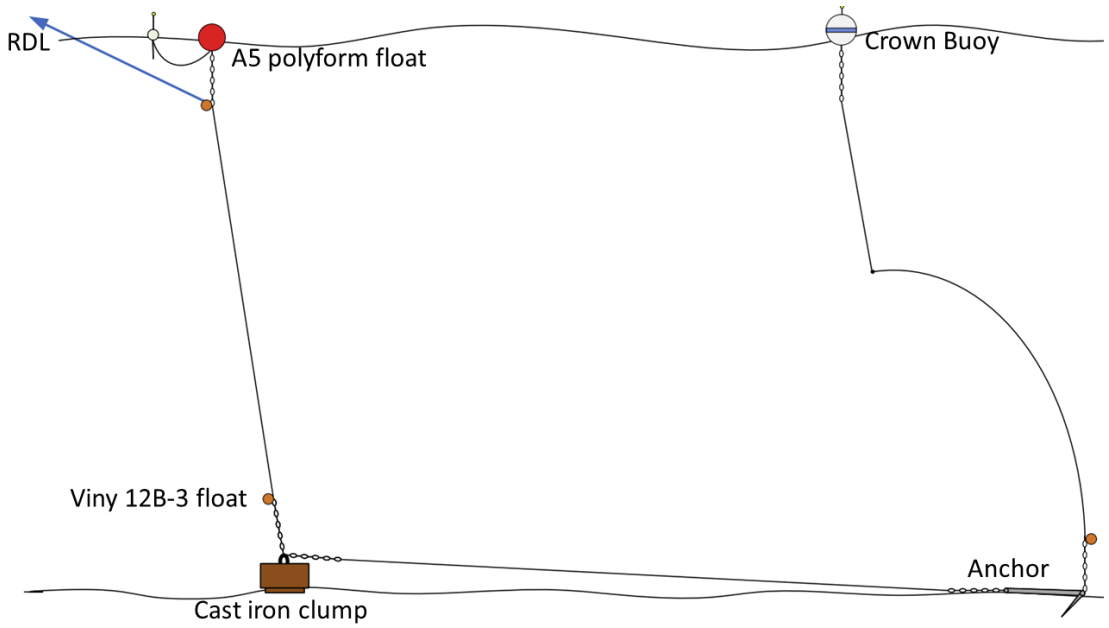

Figure 2: Annotated cartoon (not to scale) of one leg of the RDL mooring. Each mooring leg terminates at an anchor, marked on the surface by a buoy. The anchor is connected to a clump weight by a length of chain, and the clump weight is connected to the vessel by wire rope. At the end of the chain near the clump weight, there are several floats used in deployment and recovery. Note that under tension (while moored) the A5 polyform float is pulled below the surface.

The turbine was a cross-flow variant developed by the University of Washington with a rotor 1.19 m tall and 0.85 m in diameter. The rotor consisted of four straight blades with a blade chord length of 0.098 m. Four struts with cross-sections roughly matching the chord length connected the blades to the drive shaft. The rotor was coupled to a generator using an oil-filled bearing pack and a magnetic coupling. As configured for deployment on RDL, the rotor was cantilevered below the generator housing and bearing pack (Figure 3).

A downward-facing acoustic Doppler current profiler (ADCP, Nortek Signature 1000) was deployed approximately 1 m from the rotor on RDL's gantry. Two-minute running averages of horizontal velocities corresponding to depth bins approximately 1 m below the bottom of the rotor were used as a turbine control system input. Based on the average current speed, the controller regulated the rotation rate of the turbine to maintain a time-averaged tip-speed ratio (ratio of blade rotational speed to inflow velocity) of 1.8. This tip-speed ratio corresponds to the approximate maximum rotor mechanical conversion efficiency. ADCP measurements revealed minimal vertical shear in the upper water column such that a velocity measurement below the rotor plane approximated the inflow condition, while remaining unaffected by the rotor wake on ebb or flood tide.

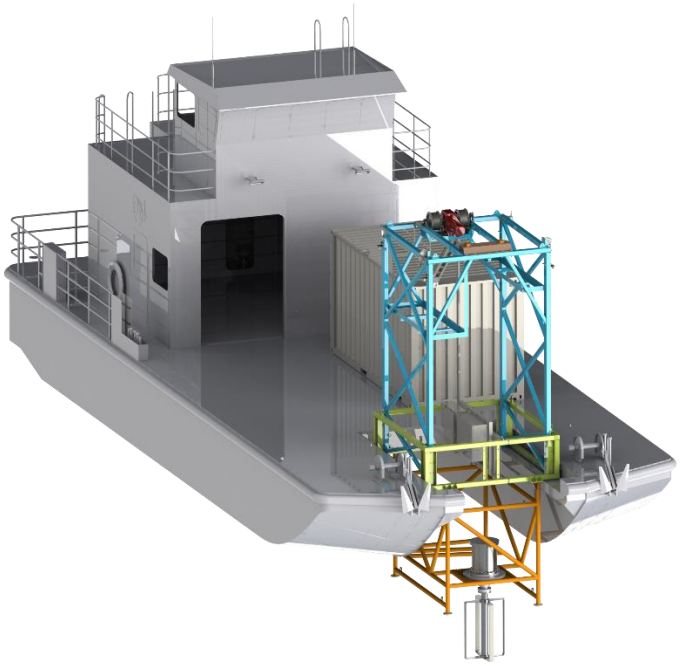

Figure 3: Model of RDL with the turbine. The turbine, suspended off the bow of the vessel, has a height of 1.19 m and a diameter of 0.85 m. The center of the rotor is ~2.06 m below the water surface.

2.2 Field Data Collection

To measure underwater noise, we used three Drifting Acoustic Instrumentation SYstems (DAISYs), the minimum number of receivers required to localize sound sources. Each DAISY includes a surface package, an underwater package, and a tether connecting the two (Figure 4). The surface package contains a GPS, compact meteorological station, inertial measurement unit, and data logger. Below the surface, coupled to the surface expressed by a 1 m rubber cord, is the noise measurement package consisting of a hydrophone (HTI 99-UHF), pressure sensor, and custom data acquisition system for logging the hydrophone voltage, pressure, and inertial measurement unit data. Each unit was also deployed with a Garmin Astro dog collar as a backup GPS to help locate the DAISY after deployment. DAISYs are designed to minimize the unwanted (non-acoustic) noise often observed in measurements in highly energetic environments (e.g., the hydrophone is surrounded by a flow shield that minimizes relative velocity during drifts).

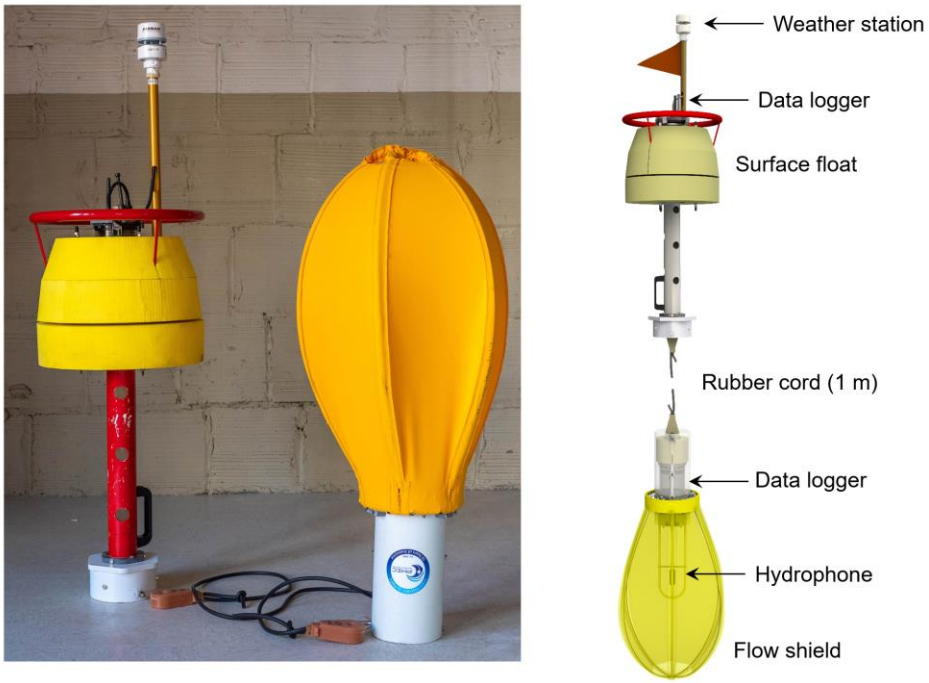

Figure 4: (left) Drifting Acoustic Instrumentation SYstem (DAISY) optimized for tidal currents. (right) Annotated system schematic. The surface package includes a weather station, data logger with integrated GPS, and surface float. Connected to the upper portion by a 1 m rubber cord, the submerged package includes a data logger, hydrophone, pressure sensor, and flow shield.

The DAISYs were deployed from R/V Sounder. While deploying DAISYs, R/V Sounder drifted with the currents to minimize relative velocity and, following release, moved to a standoff distance and shut down all vessel systems to avoid contaminating the acoustic measurements. DAISYs were released upstream of RDL (to the north during the flood tide), drifted past RDL and the turbine, and were then recovered once all units had passed out of the survey area. Because of the risk of mooring entanglement, the DAISY drifts had to maintain a minimum standoff distances on the order of 50 m from RDL. A set of representative DAISY trajectories is shown on Figure 1.

To localize sounds originating from RDL and the turbine–and to investigate changes in radiated noise with inflow velocities and operating conditions–five drifts were conducted during the flood tide. During each drift, two DAISYs were deployed to pass RDL on the port side (weaker currents), and one was deployed on the starboard side. For each drift, means and standard deviations of DAISY speed over ground, wind speed measurement by one unit's meteorological station, and hydrophone depths were calculated from track metadata (Table 1).

Table 1: Track metadata for DAISYs deployed around *R/V Russell Davis Light* in Agate Pass

Localization Drift	DAISY No.	Speed over Ground [m/s]	Wind Speed [m/s]	Hydrophone Depth [m]
A	1	1.20 ± 0.07	0.9 ± 0.5	2.38 ± 0.02
	2	0.21 ± 0.07	-	2.38 ± 0.01
	3	0.70 ± 0.12	-	2.34 ± 0.02
B	1	0.69 ± 0.05	0.4 ± 0.2	2.38 ± 0.01
	2	1.30 ± 0.08	-	2.15 ± 0.01
	3	0.6 ± 0.16	-	2.35 ± 0.01
C	1	1.4 ± 0.14	1.2 ± 0.5	2.38 ± 0.01
	2	0.86 ± 0.08	-	2.37 ± 0.01
	3	0.72 ± 0.02	-	2.35 ± 0.01
D	1	0.72 ± 0.08	1.6 ± 0.6	2.38 ± 0.01
	2	1.00 ± 0.07	-	2.38 ± 0.01
	3	1.5 ± 0.09	-	2.35 ± 0.01
E	1	1.6 ± 0.12	0.9 ± 0.5	2.38 ± 0.02
	2	1.10 ± 0.10	-	2.37 ± 0.02
	3	0.99 ± 0.10	-	2.35 ± 0.01

To benchmark the effectiveness of the DAISY localization protocol, we employed a “cooperative” source with known timing and origin. Several times during localization drifts, one of the co-authors aboard RDL hit the deck with a steel pipe to create an impulsive sound. Although the noise had to propagate through the vessel and into the water, thus creating ambiguity in the source location, this approach provides some spatial constraints on the approximate source location (i.e., successful localization should fall within RDL’s footprint).

2.3 Dockside Test

Prior to testing in Agate Pass, we took acoustic measurements of the turbine in a dockside setting to predict the types and intensities of sound that might be detectable in the field. Tests were conducted on 23 March 2022 while RDL was at the University of Washington Applied Physics Laboratory dock in Portage Bay (Seattle, WA). The turbine was submerged to the same depth as in Agate Pass and motored by the generator from 60 to 110 rpm in increments of 5 rpm, a broader range of conditions than would later be experienced in Agate Pass. Speed, torque, and power data from the turbine system were recorded throughout the test, including when the power electronics and generator were energized and de-energized.

During these tests, a hydrophone (OceanSonics icListen HF) was positioned at a depth of 3 m and 2.5 m away from the axis of rotation. While vessel traffic was limited throughout the test, the dock is located directly under a bridge with heavy vehicle traffic. Prior measurements indicated relatively high levels of ambient noise at the dock due to this traffic and other anthropogenic noise sources along the highly developed urban shoreline.

2.4 Data Analysis

2.4.1 Acoustic Data Processing

Hydrophone time series data were used to calculate multiple acoustic data products. First, raw time series data were split into 1-second windows (N = 512,000 points) with 50% overlap. These were tapered using a Hann window and processed using frequency-dependent calibrations to generate pressure spectral densities (PSD) with 1 Hz resolution. To reduce data volumes, variable band merging was used to calculate hybrid milli-decade levels (Martin et al. 2021a, 2021b), which have 1 Hz resolution below 435 Hz and lower resolution corresponding to 1/1000th of a decade (order of magnitude increase) at higher frequencies.

2.4.2 Extrapolation of Dockside Data to Field Site

Dockside sound generated while motoring the turbine power take-off was extrapolated to measurements at Agate Pass to inform comparisons between potential radiated noise from the operating rotor and ambient noise. Assuming that the power-take off produces similar radiated noise during power generation and motored operation, dockside acoustic data are used to predict received levels at Agate Pass using a hybrid spherical/cylindrical spreading model with negligible absorption. The PSD of turbine noise expected to be received by a DAISY is estimated as $PSD_{DAISY} = PSD_{dockside} - 15\log_{10}\left(\frac{r_{DAISY}}{r_{dockside}}\right)$, where subscripts denote location and r is the distance between the turbine and DAISY.

2.4.3 Localization

The goal of localization is to estimate the origination location of a signal to aid in source attribution. Localization requires knowledge of the location and geometry of the receiver array, as well as the ability to temporally resolve signals of interest. To perform a two-dimensional localization, at least three receivers are required. Here, we implement a time-difference-of-arrival (TDOA) technique on signals of interest identified in manual review. For example, Figure 5 shows received levels from the cooperative source on the three DAISYs in the drift, as well as the time and frequency ranges of interest. In this approach, the locations of the receivers—the three DAISYs—and the differences in the arrival time of the signal at each are used to estimate the source location.

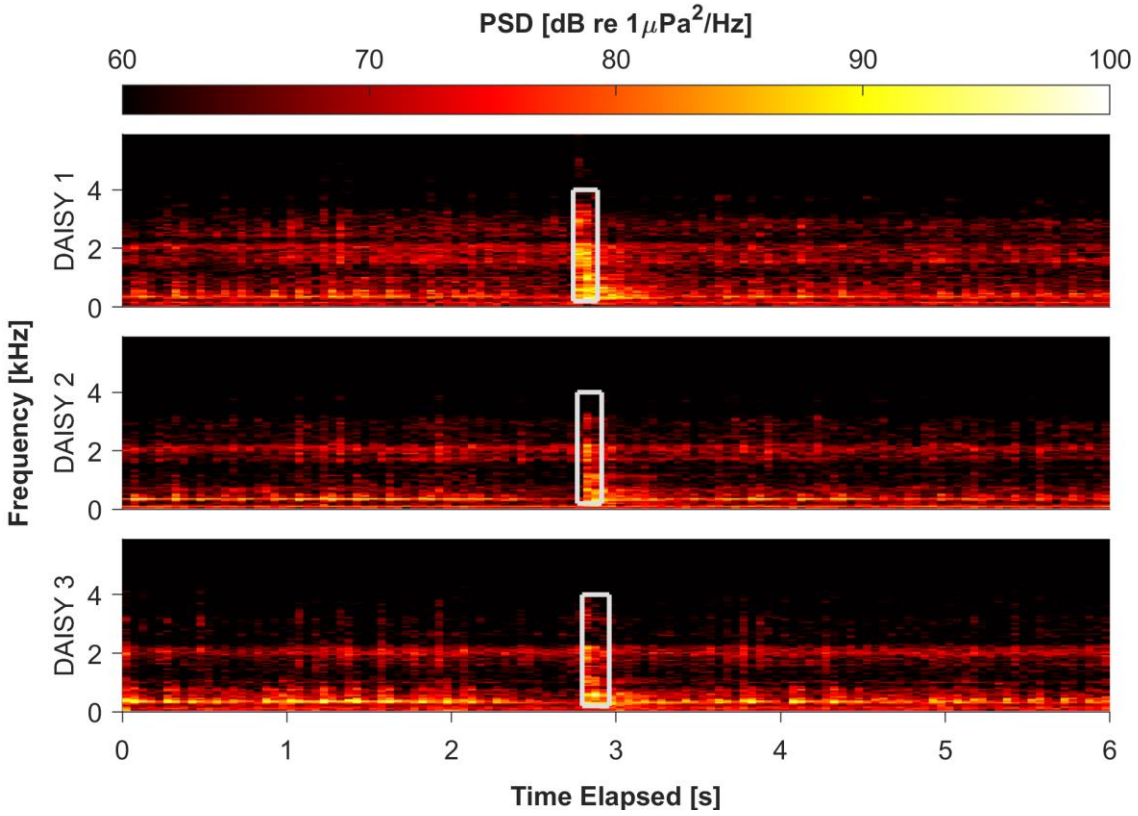

Figure 5: Spectrograms showing simultaneous received levels from the three DAISYs during a portion of Localization Drift 3. A cooperative strike is visible as an impulsive, broadband signals at ~3 s. White boxes denote the frequency and time ranges chosen for the strike to localize its source.

The first step in localization is to identify the arrival time and frequency ranges corresponding to signals of interest in each of the co-temporal DAISY tracks. For each event, we detrend the hydrophone voltage and apply a bandpass filter (typically ~200 – 4000 Hz) to suppress noise outside of the band of interest (Figure 6). In each event time series, the index of the maximum absolute value of the cross-correlation is taken as the reference time of arrival. By using the same portions of the time series on all units, the indices associated with the peak in the cross-correlation correspond to the time delay between the signals with added uncertainty introduced by complex propagation (multipath arrivals) and ambient noise.

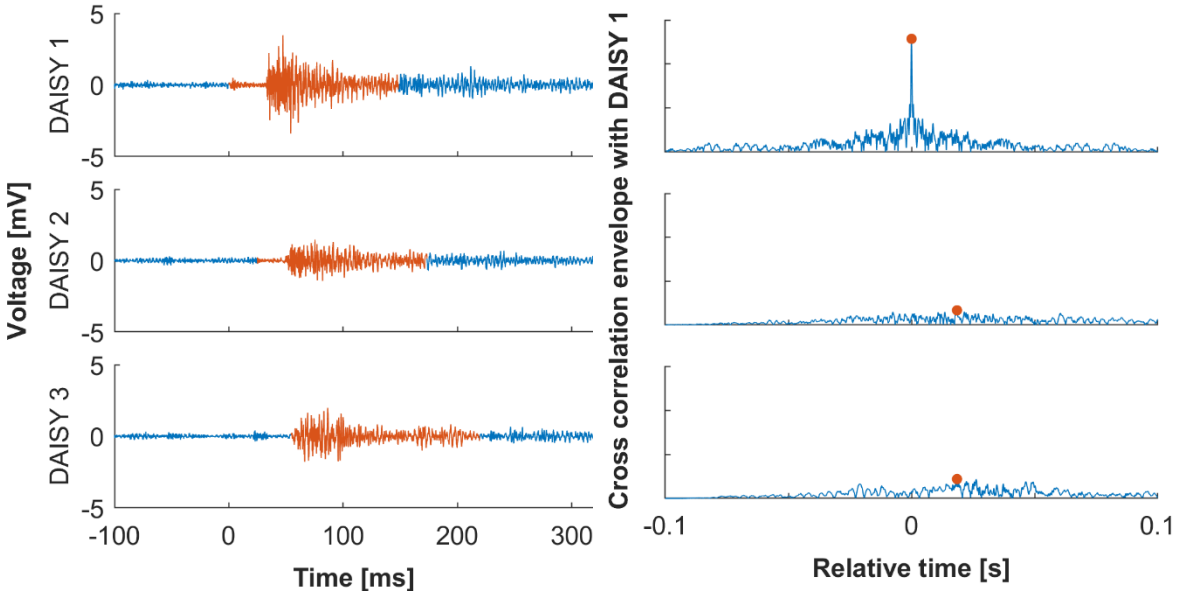

Figure 6: Intermediate localization results for a cooperative strike in drift C. (left) Hydrophone voltage around the strike after it has been de-meaned and bandpass filtered to the frequency range of the strike sound (200-4000 Hz). The orange portion denotes the duration of the signal that is considered part of the event. (right) Auto-correlation of DAISY 1's signal and its cross-correlations with the other two DAISYs. The blue line is the envelope of the value of the cross-correlation, and the orange dot marks the point with the highest value. The relative time of this point is considered the time of arrival of the strike.

With these arrival times, we apply a TDOA localization method (Sayed et al. 2005, Guido 2014) to estimate the source location. Sound speed profiles show that the water column was well mixed throughout the measurement period, with a speed of sound of approximately 1480 m/s at DAISY depth. We can estimate the difference in the distances between the source and the i_{th} DAISY and the source and the j_{th} DAISY as

$$r_i - r_j = (t_i - t_j)c, \qquad \text{(Eq. 1)}$$

where r is the distance from the source to the subscripted DAISY, t is the reference time for the event, and c is the speed of sound in water (assumed constant for all DAISYs).

Using the difference in distance to the source for each pair of DAISYs, the source position can be calculated as a function of the distance from the closest DAISY (i.e., the first DAISY to receive the signal) to the source. This DAISY becomes the reference ("receiver 1") for the event analysis and, with three receivers, the source position as a function of the distance to the reference is given as

$$\begin{bmatrix} x_s \\ y_s \end{bmatrix} = \begin{bmatrix} x_2 & x_3 \\ y_2 & y_3 \end{bmatrix}^{-1} \left(r_1 c \begin{bmatrix} t_1 - t_2 \\ t_1 - t_3 \end{bmatrix} + \frac{1}{2} \begin{bmatrix} {x_2}^2 + {y_2}^2 - c^2(t_2 - t_1)^2 \\ {x_3}^2 + {y_3}^2 - c^2(t_3 - t_1)^2 \end{bmatrix} \right), \qquad \text{(Eq. 2)}$$

where x and y are the easting and northing positions. For the DAISYs, position is relatively well constrained by their surface expression GPS (accuracy of ±2 m). Finally, substitution of this intermediate result—the source coordinates in terms of r_1—into the geometric definition of r_1,

$${r_1}^2 = (x_1 - x_s)^2 + (y_1 - y_s)^2, \qquad \text{(Eq. 3)}$$

yields a second-order polynomial. The largest real root of this polynomial is taken as r_1 and, from this, the location of the source can be identified using (Eq. 2).

3 Results

3.1 Dockside Test

Three notable features are apparent in measurements from dockside testing (Figure 7). First, when the system is powered and rotating, there is a notable tone at 8 kHz, which we attribute to the power electronics due to the relatively high frequency and the frequency invariance with rotation rate. Second, when the motor is powered on, a tone at approximately 4 kHz is present regardless of the rotor's rotation. The observed noise in this band varies as a function of rotation rate with broader spread between observed tones in the 3.9-4.1 kHz band as the rotation rate increases. Lastly, there are multiple tones generated in the 100 to 400 Hz range that are dependent on the rotation rate. The frequency of the highest intensity tone is strongly correlated with rotation rate (Figure 8a). In contrast, the intensity of the tone is not well correlated with rotation rate or power input to the rotor (Figure 8b).

3.2 Field Measurements

Five total drifts were conducted, but here, we focus on a single track, which had the highest signal-to-noise ratio and is therefore the most likely to reveal noise from the operating turbine. Measurements from Agate Pass (Figure 9) suggest that there are three main differences between the field measurements and dockside testing. First, the soundscape in Agate Pass during turbine operation (Figure 9) differs from the dockside tests (Figure 7), with higher levels of ambient noise over most frequencies. While somewhat surprising given the noisy environment of dockside testing, we attribute this, in part, to noise produced by RDL itself. Second, turbine operation also differs, with the rotor being driven by the currents (experiencing a thrust load absent in the dockside testing) and with rotation rates varying with inflow conditions. Third, the Agate Pass measurements were taken at a greater distance (Figure 9e). Due to these differences, over short periods of time (e.g., minutes), signals measured from the turbine in Agate Pass would not be expected to vary to the same extent nor be as prominent as those from dockside testing. However, the anticipated radiated noise signals from the turbine were not observed in Agate Pass. It is unclear whether this is directly attributed to masking by ambient noise or to differences in the radiated noise from the turbine under load. The 8 kHz tone from the servomotor was present, but only exceeded ambient noise at the beginning of the drift track (Figure 9b), and there was no discernible servomotor tone at 4 kHz (Figure 9c). At frequencies below 400 Hz, there are multiple signals present, including many narrowband tones with constant frequency. Since the rotor rotation rate was nearly constant, one might presume that these are attributable to the turbine rotor. However, at the predicted frequency for the driveline, only a relatively low intensity tone (170-175 Hz) during the initial part of the drift, was observed (Figure 10).

In summary, though the dockside test provides useful information for analysis of data collected in Agate Pass, the conditions—and resulting acoustics—at these two sites are disparate. The absence of anticipated sounds in the Agate Pass data could be attributed to two factors. First, the turbine could be producing a different sound in Agate Pass than during dockside testing because of the different operating mode (power generation under thrust versus motored, respectively). However, we believe that a second factor dominates. Namely, that the same signals are produced by the turbine, but the higher ambient noise in Agate Pass and lower received levels reduce the signal-to-noise ratios and mask the turbine signal at the measurement distance. Extrapolation from the most intense signal in the driveline noise range of the dockside data (Figure 8a) suggests that the inflow velocity during the drift shown in Figure 9 and Figure 10 would result in driveline noise at a peak of approximately 109 dB re 1μPa^2/Hz at a range of approximately 2 m in the Agate Pass measurements. During this drift, measured ambient noise around the peak predicted frequencies (170-175 Hz) is approximately 65 dB re 1μPa^2/Hz (Figure 9d). Thus, based on transmission losses and motor/generator assumptions, one might expect to observe rotor noise to a range of approximately 850 m without accounting for signal-to-noise ratios. The DAISY stayed within this range (Figure 9e) and therefore should have measured rotor noise well above the ambient noise threshold for the entirety of the drift. However, there are only marginal indications of this sound at the beginning of the track (Figure 10), and they never exceed 80 dB re

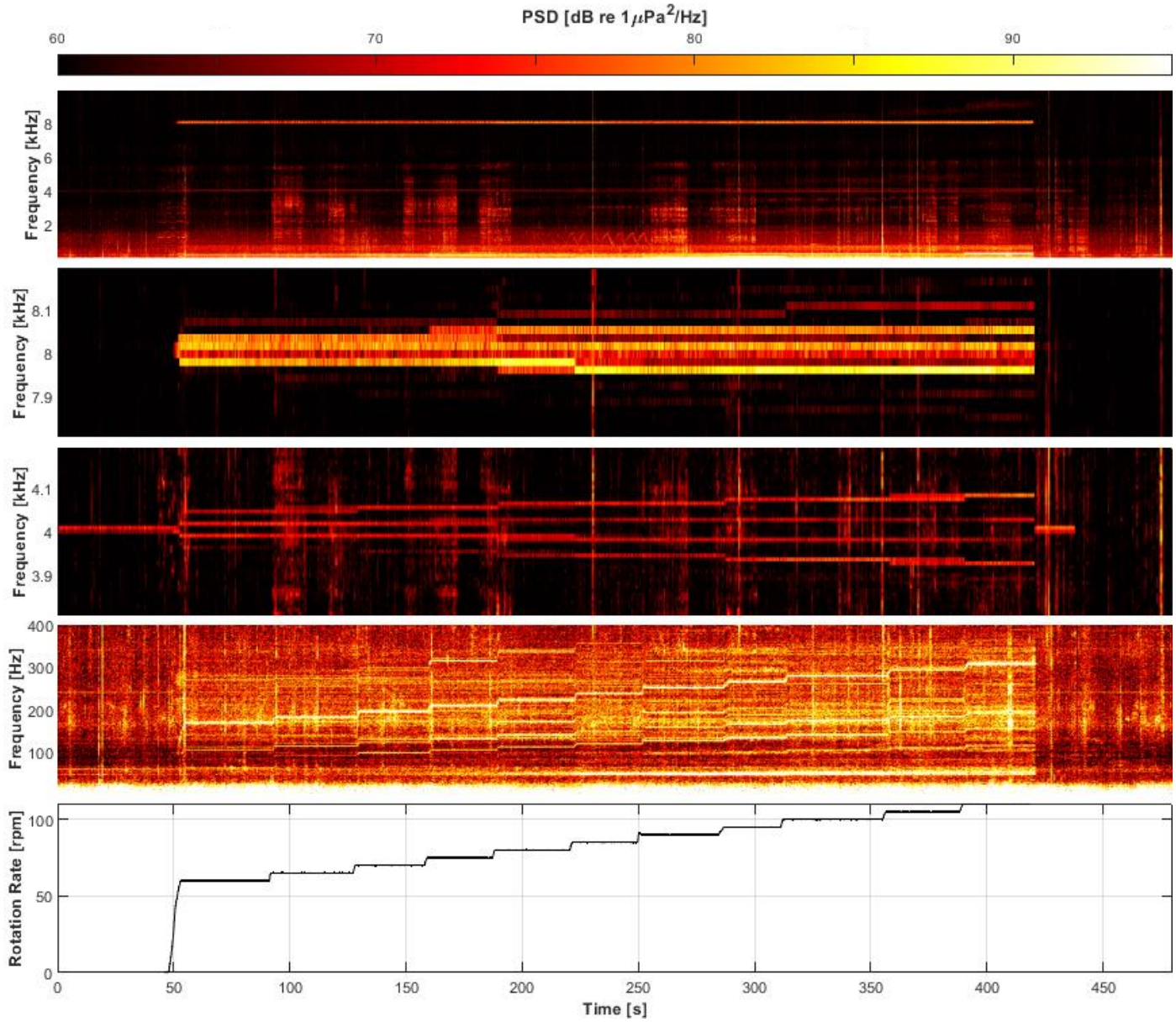

Figure 7: Measured noise during dockside turbine testing. The turbine rotates from 50-390 s and the servomotor is energized from 0-440 s. (a) Spectrogram over all frequencies of interest. Noise is most intense below 2 kHz. Once turbine rotation begins, intensity increases below 1 kHz, at 4 kHz, and at 8 kHz. (b) The spectrogram centered on 8 kHz shows a 7950-8100 Hz tone during turbine rotation, attributed to the power electronics. (c) The spectrogram centered on 4 kHz shows a 3900-4100 Hz signal while the servomotor is energized and is, therefore, attributed to the servomotor. Once turbine rotation begins, the signal bifurcates into four tones with increasing separation as the rotation rate increases. (d) The 0-400 Hz spectrogram shows multiple tones that increase in frequency with rotation rate. (e) The rotation rate increases by 5 every 20-50 seconds, creating a step signal.

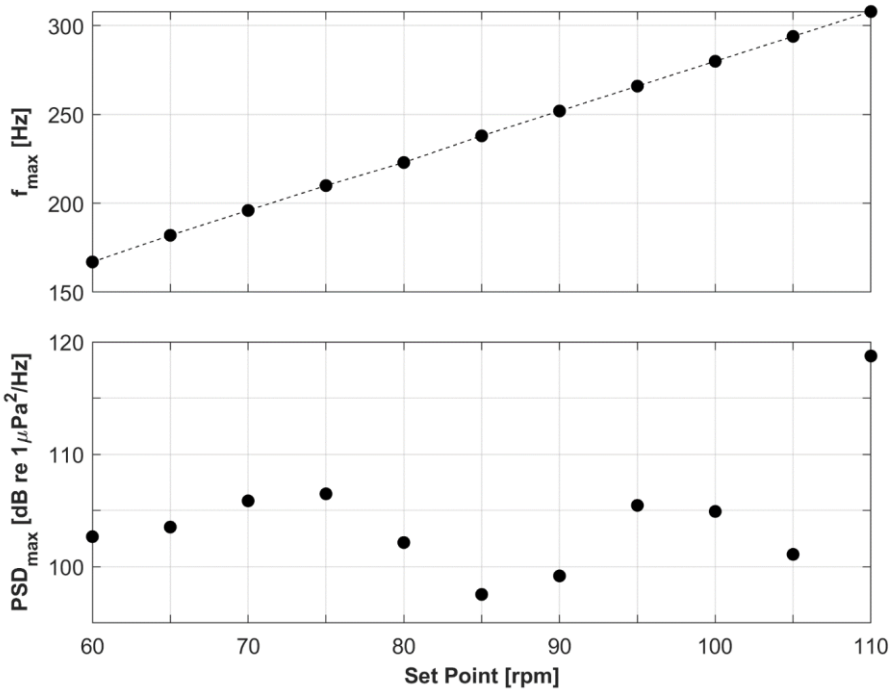

Figure 8: (top) Regression of frequency of maximum PSD in the 100 – 400 Hz range (rotor noise) against turbine rotation set point shows a linear relationship between rotation rate and frequency of peak tone. (bottom) Maximum PSD in the 100 – 400 Hz range as measured at range of 2.5 m from the axis of rotation of the turbine shows no clear dependency on rotation rate.

1µPa2/Hz. This suggests that the intensity of the driveline noise changes with rotor thrust loading or that our spreading model under-predicts transmission loss between the source and the receiver. Similarly, indications of the power electronics noise around 8 kHz (Figure 9b) are lower intensity relative to the prediction, consistent with the hypothesis of higher transmission loss.

In general, ambient noise poses the greatest challenge to definitively attributing sounds to the turbine at frequencies below 3.5 kHz. In particular, the band where we had anticipated rotor noise overlaps with a variety of sound sources (Figure 11) not present in dockside testing, including contributions from RDL's generator, intermittent signals (subsequently attributed to RDL's moorings), and vessel traffic. The rationale for these attributions are now discussed.

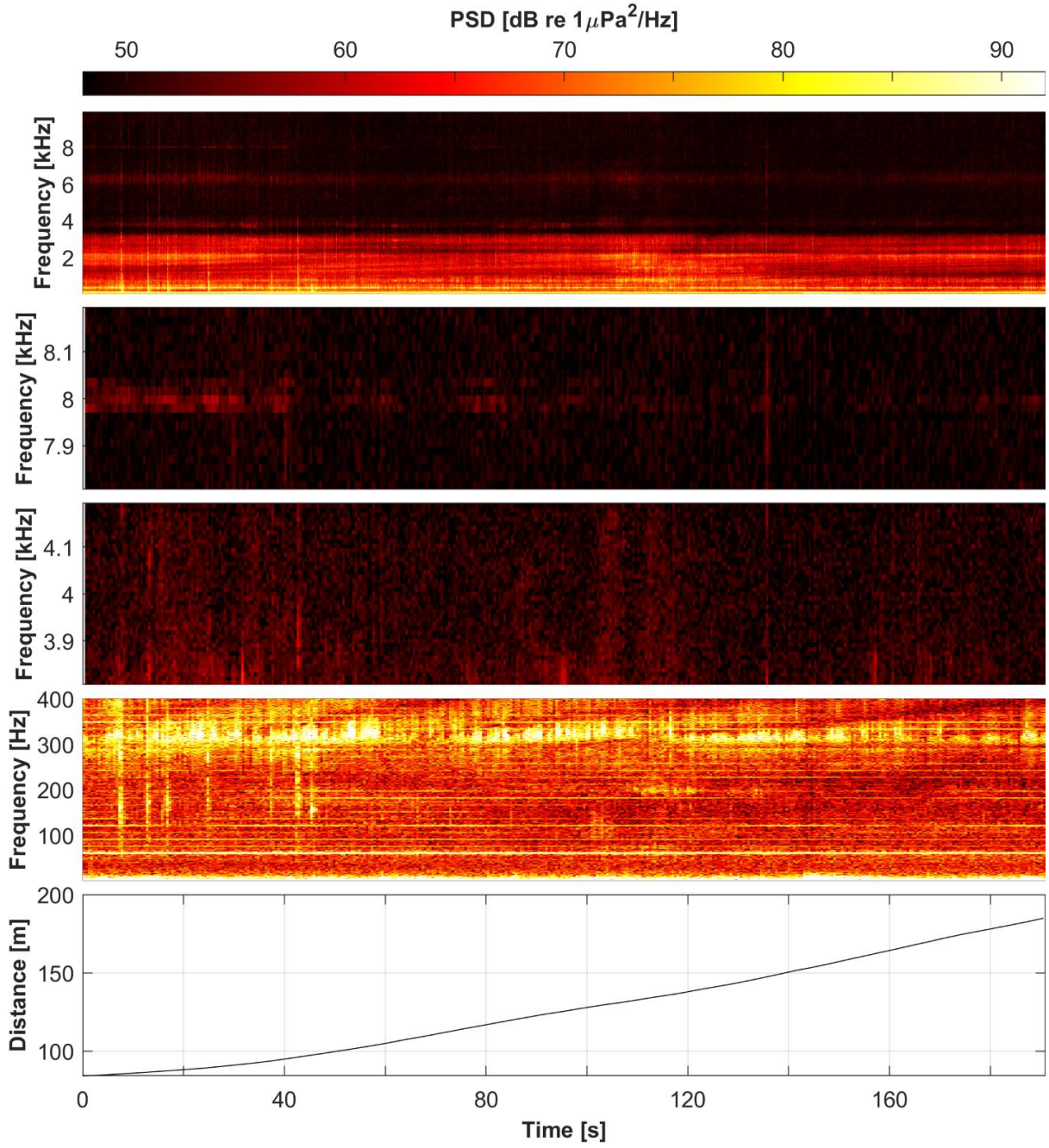

Figure 9: Measured noise during track C1, presented in the same frequency bands as for dockside testing to highlight presence/absence of turbine-attributed sound. During this drift, the turbine's rotation rate varied from 61-63 Hz. a) Spectrogram over all frequencies of interest, demonstrating that noise is most intense at frequencies below 3.5 kHz. (b) The spectrogram centered on 8 kHz shows a faint band of sound, apparent above ambient noise for the first 40 s of the track, that is attributed to the servomotor. (c) Unlike during dockside testing, the spectrogram centered at 4 kHz (expected servomotor sound) does not contain any narrowband signals. (d) The spectrogram from 0 – 400 Hz has multiple signals, including persistent narrowband and impulsive broadband signals. (e) The distance between the DAISY and the turbine steadily increases as the DAISY drifts with the dominant currents. The weaker servomotor signal (b) is correlated with increasing distance between source and receiver.

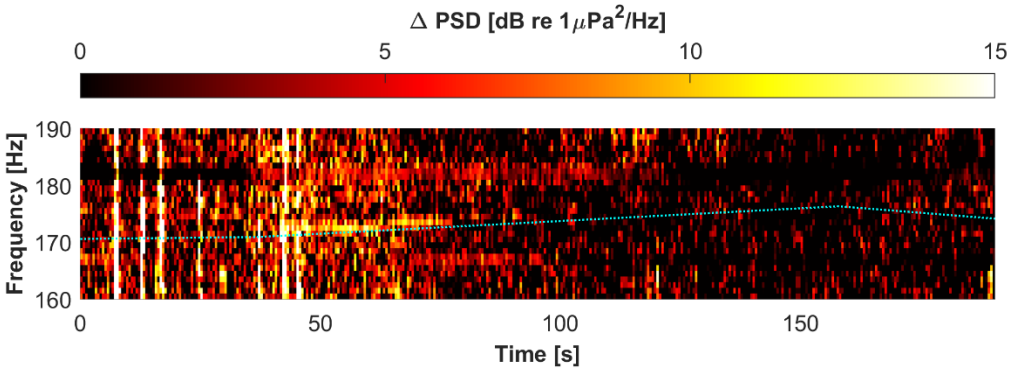

Figure 10: Normalized spectrogram highlighting anticipated turbine driveline noise from dockside testing (160-190 Hz) for the same period shown in Figure 9. This formulation shows the difference in PSD from the median PSD for each frequency, removing noise that persists across time at constant frequency. This aids in identification of low SNR horizontal banding structure (e.g., at approximately 165 Hz and 180 Hz in Figure 9), which is attributed to RDL's generator. The dotted cyan line reflects our prediction for the frequency of turbine rotor sound based on operating state and DAISY-turbine separation distance. There is increased intensity along this trajectory from ~40-80 s, which might be attributable to the turbine and overlaps with the period during which the servomotor sound is detected. For most of the drift, there is no sound above ambient at the predicted frequency.

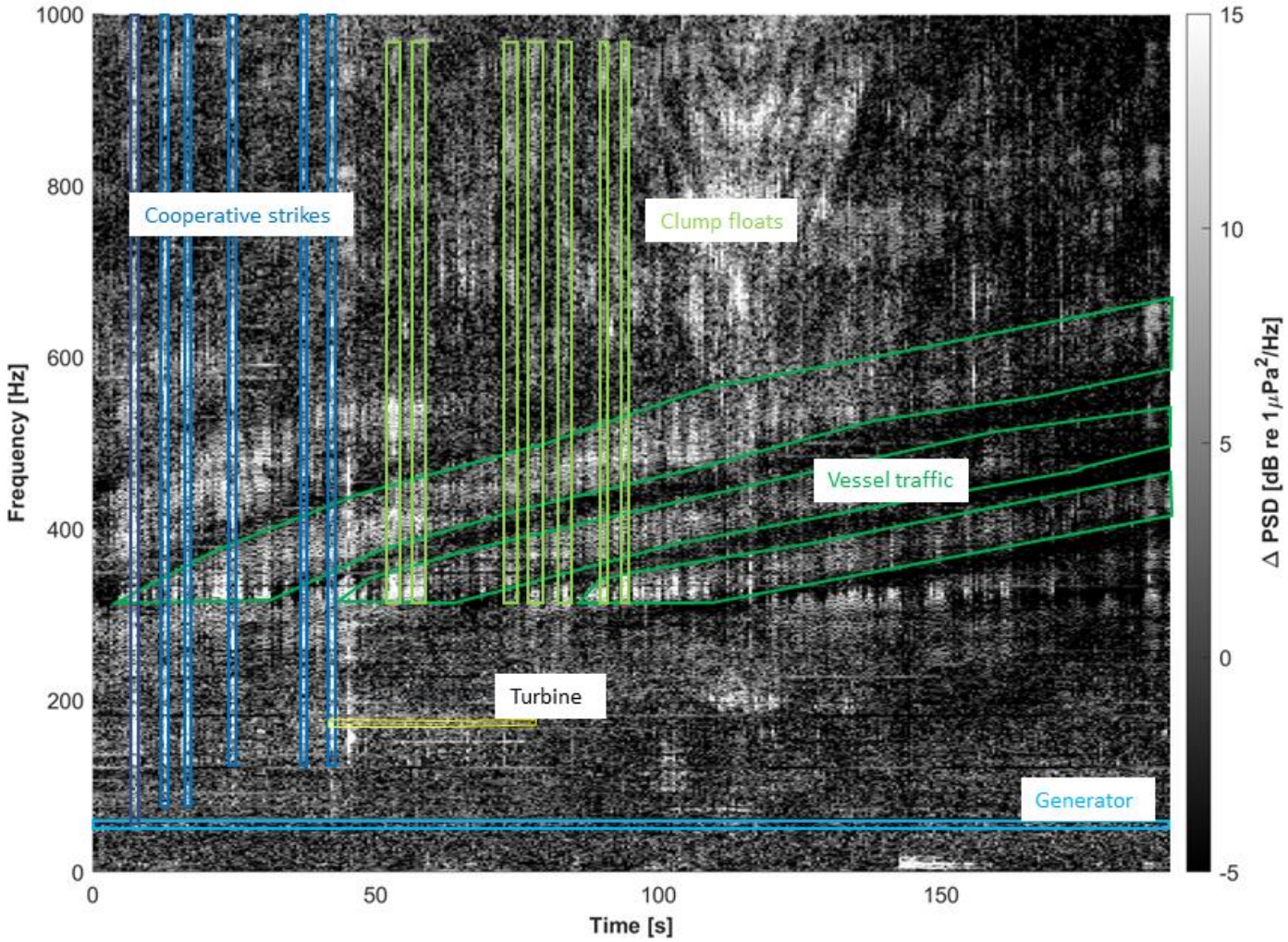

Figure 11: Soundscape from 0-1 kHz for track C1 with representative annotations denoting attributed sources—the turbine driveline (low certainty), RDL generator, cooperative strikes, clump floats, and vessel traffic. As a relative spectrogram, this visualization emphasizes signals that change over time. Noises attributed to the generator presents as a constant set of, narrow band signals that occur every 15 Hz, starting at 60 Hz. Relative PSD was chosen for visualization to prevent the generator signals from dominating the figure. Because they are relatively consistent in time, they appear as approximate nulls in the relative spectrogram. Limited noise attributed to the turbine driveline sound is visible, ~170 Hz from 40-80 s. Cooperative sounds created for testing appear as impulsive, broadband signals at the beginning of the drift. A series of impulsive 300-1000 Hz tones are attributed to clump floats on the RDL mooring. Finally, the diagonal bands of increased intensity are attributed to another vessel underway.

Of the ambient noise sources identified, the tones we attribute to the RDL generator (Figure 11) overlap the most with the predicted rotor noise frequency range. The main tone we attribute to the generator is a strong, narrowband tone at 60 Hz present in all drifts, with strong harmonics of this tone every 60 Hz (Figure 12). There are also less intense tones every 15 Hz starting at 75 Hz and extending to at least 1270 Hz where their intensity drops below the ambient noise floor. These can be attributed to the generator because of their frequency, consistency over time, and changes in intensity with location. The generator has two pole pairs and rotates at 1800 rpm. The frequency associated with this is given by the product of the rotation rate (in cycles/second) and the number of pole pairs, which, for this specific generator, is 60 Hz. Since the rotation rate remains constant, signals from the generator should not modulate in frequency, which is consistent with observations. Additionally, the 60 Hz tone is most intense near the port (west) side of the vessel (Figure 13), which is where the RDL generator was located. We note that localization (subsequently used to identify sound from the mooring) would be complicated by the consistency of this noise over short timescales (i.e., drift duration) and the long baseline of the DAISYs so is not employed here.

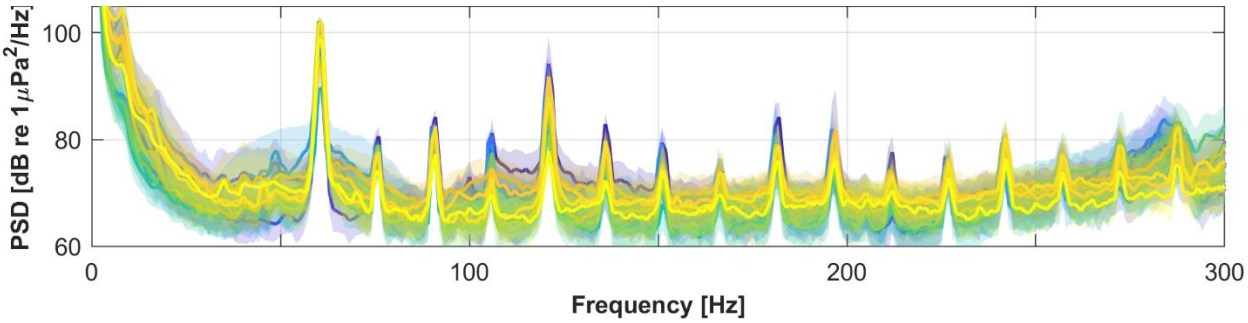

Figure 12: Composite periodograms of all tracks for the duration of their drifts. Each colored line represents the mean intensity at each frequency for a track with the translucent regions encompassing the 25-75th percentile. Starting at 60 Hz, all of the tracks have harmonic peaks every 15 Hz. These originate from the 60 Hz tone associated with the fundamental frequency of the RDL generator due to its rotation speed and number of pole pairs.

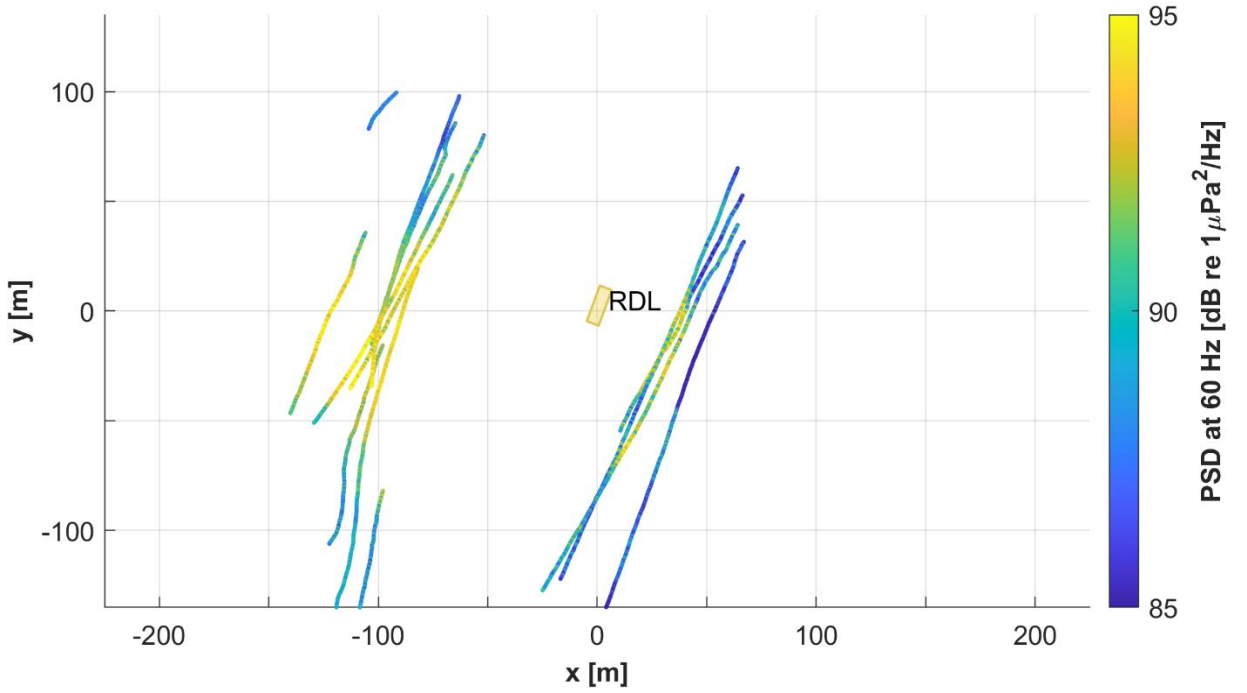

Figure 13: Spatial variation in intensity of the 60 Hz tone. The color of each track denotes the PSD at 60 Hz along a DAISY trajectory. The intensity is highest to the west of RDL, which corresponds to the location of the generator exhaust port.

As the generator signals are mostly consistent across time, they can be filtered for visualization by subtracting the median value (e.g., Figure 10). However, this strategy cannot be utilized in drifts where the rotor noise frequency is predicted to intersect with a generator frequency. For example, in the drift shown in Figure 14 the turbine is expected to produce sound at a frequency of 145-150 Hz. This overlaps with a generator harmonic at 100 s, likely masking any potential rotor sound during this period. In addition to the generator, other sound sources present in the dataset include another vessel and impulsive broadband sounds, which we attribute to cooperative testing and to the moorings (Section 3.3.3).

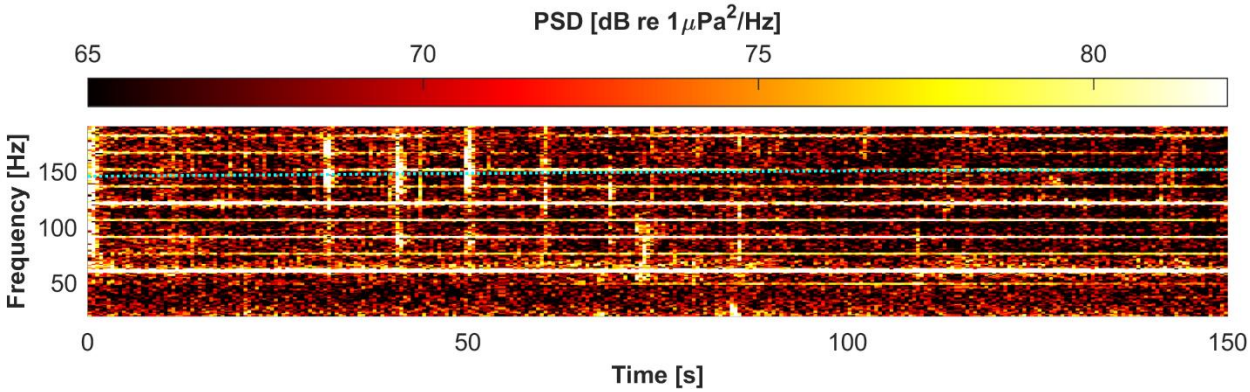

Figure 14: The spectrogram for track B1 shows the relatively intense signals attributed to RDL's generator. In addition to the primary tone at 60 Hz and first harmonic at 120 Hz, lower intensity peaks every 15 Hz are observed starting at 75 Hz. The harmonic at 150 Hz intersects the predicted turbine rotor sound frequency (dashed cyan line) at about 100 s, masking potential turbine rotor noise.

3.3 Source Localization for Attribution

As discussed in Section 2.Localization, the cooperative noises created by striking the RDL deck with a pipe create clear, broadband, impulsive signals. These could be easily attributed based on their known timing, but also serve as a test for localization methods. As shown in Figure 15, the strikes generally localized to within 20 m of RDL's location. This is indicative of the effectiveness of the overall localization strategy for sufficiently high signal-to-noise ratios (SNR) with the minimum number of required receivers. We note that given that the strike noise is radiated by the hull, the "point" source size is relatively large and on the same order as vessel size.

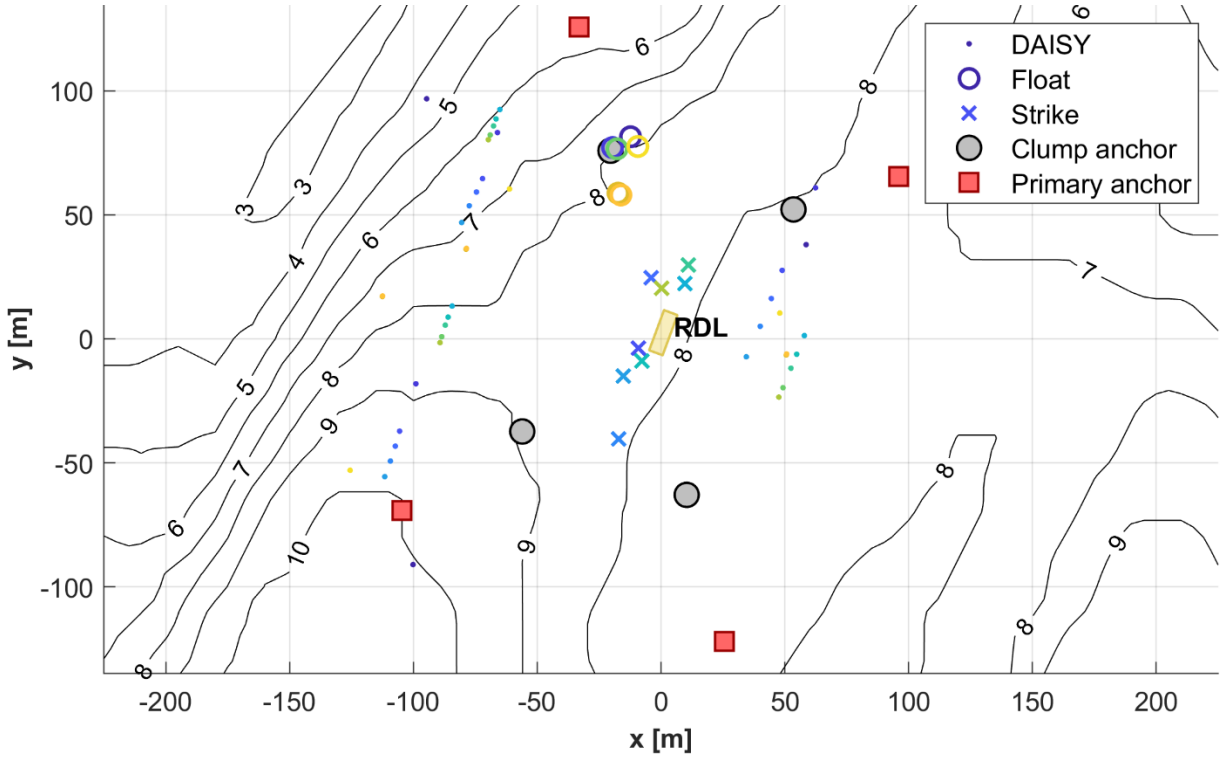

Figure 15: Composite localization results for all drifts. For each localized sound, there are three dots marking the locations of the three DAISYs at the time of the signal. The estimated location for the sound source is marked in the same color. The cooperative strike localizations are all within 50 m of RDL (all but one within 20 m). The float noise localizations are all within 20 m of the NW clump weight.

Similarly, we can employ localization to identify the source of the recurring sound between 300 and 1000 Hz (Figure 11, highest intensity in the 300-550 Hz range) that is present in all drifts. Localizations of several instances of this sound all produce results in the vicinity of the NW clump weight (Figure 15). Noise levels observed in the 300-550 Hz band are also highest in this region (Figure 16). These suggest that the sound is attributable to the clump weight. The sound presents as tapping, which we hypothesize to originate from periodic contact between the floats located near the clump weights on this specific leg of the mooring.

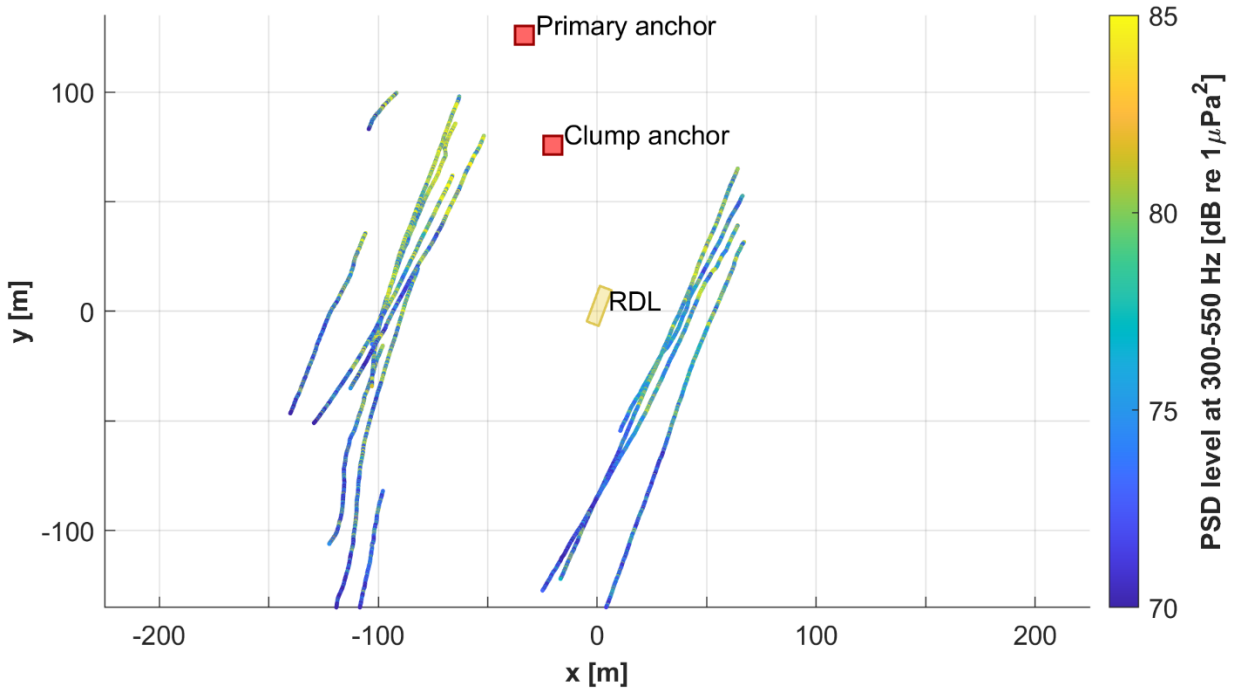

Figure 16: Spatial variation in intensity in the 300-550 Hz band across all drifts shows that this band is dominated by the periodic signal that is most intense in the vicinity of the NW clump weight.

4 Discussion

The DAISY measurements demonstrate both the relatively small acoustic footprint associated with the turbine and the complexity of obtaining high-quality measurements under the test conditions. Rotor driveline noise could not be identified with high confidence, demonstrating that radiated noise from the system does not consistently exceed ambient spectral levels at these low frequencies (~65 dB re 1µPa^2/Hz at 130-180 Hz). Constituents at 4 and 8 kHz, attributed to the servomotor and power electronics, respectively, could be identified. However, at ranges of 40-150 m from the source, these signals had minimal SNRs (~6 dB), making them difficult to detect at larger ranges. Thus, across the entire range of measured frequencies, we only observed minor contributions to noise from the operating turbine.

In dockside testing, we were able to identify noise from the driveline (100-400 Hz), servomotor (~4 kHz), and power electronics (~8 kHz). There was a strong correlation between the rotation rate of the turbine and the frequency of the turbine noises, particularly in the driveline frequency range. However, there was no obvious correlation between the rotation rate and the intensity of the noise. Although we could not confidently identify driveline noise in our field data, the servomotor and power electronics noises

both presented in the field at the same frequency ranges as in dockside testing. Dockside extrapolation was a valuable tool for identifying these signals in the much lower SNR field data. In future work, if driveline noise were observable, we recommend repeating dockside testing and comparing the driveline noise predictions to the field results.

Although we were not able to attempt localization of any turbine sounds due to low SNR and signal ambiguity, other sounds were successfully localized despite the challenging, shallow-water environment. The cooperative sounds created by striking the RDL deck provided useful information about the accuracy of our localization methods. Most of the strikes localized to within 20 m of their source location. We attribute a portion of the localization error in these results to propagation of the strike sound through the metal hull, which is unlikely to act as a point source. In addition, the shallow water environment produces complex multi-path arrival structures with relatively small differences in arrival time, which makes identifying the precise signal arrival time more complex. This ambiguity will be decreased in situations with deeper water. Localization accuracy would also increase with an over-determined array of receivers (i.e., more than three DAISYs). In addition, we are continuing to develop alternate algorithms and improvements to more precisely identify arrival times.

Based on the strength of our results for the cooperative sounds with a known source location, we were able to use localization to identify unknown signals. We hypothesized that the 300-550 Hz tapping sound which persisted throughout the acoustic data came from mooring floats. Localization supported this hypothesis and attributed the sound specifically to clump floats on the NW mooring. Despite the lower SNR, these tapping sounds localized to a more precise area than the cooperative strike sounds did, most likely due to the smaller size of the source (the clump anchor floats v. the RDL hull). In addition to eliminating this sound as a possible turbine sound, these results tell us specifically which part of the mooring could be fixed or improved for future deployments to minimize noise.

In summary, the turbine did not produce a detectable acoustic signal and thus did not contribute a significant amount of noise relative to ambient conditions. Some of the ambient noise came from the vessel and its mooring, so in future operations, when the turbine is deployed on a gravity foundation, it should be easier to identify turbine signals. Localization, even in these shallow waters, has been demonstrated successfully and will be a valuable tool in future research. Further work on the subject should explore different arrival time algorithms that may reduce uncertainty.

5 Conclusions

Underwater noise measurements using Drifting Acoustic Instrumentation SYstems (DAISYs) were conducted on April 20, 2022 around a cross-flow turbine deployed from R/V Russel David Light (RDL) in Agate Pass, Washington. Measurements were collected from the same turbine suspended from a dock and manually motored on March 23, 2022 in Seattle, Washington. Dockside testing revealed sounds created by the driveline, servomotor, and power electronics of the turbine with a frequency dependence on the rotation speed. At Agate Pass, the dockside data was used to identify signals from the servomotor and power electronics, but no significant driveline noise above ambient could be identified. There were no turbine signals with a high enough signal-to-noise ratio to localize, but both intentionally created sounds from strikes to the RDL deck and unexpected sounds from the RDL mooring were localized with accuracy. We expect localization accuracy to improve in deeper, more favorable propagation environments—like Sequim Bay, Washington, where we will repeat acoustic measurements of the same turbine with bottom-mounted hydrophones in Spring 2023—, with changes in the signal time-of-arrival identification algorithm, and a larger number of receivers. Both dockside testing and

localization proved useful for determining which signals could and could not be attributed to the turbine.

6 References

Bassett, C. and Polagye, B. (2020) Risk to marine animals from underwater noise generated by marine renewable energy devices, in OES-Environmental 2020 State of the Science Report: Environmental Effects of Marine Renewable Energy Development Around the World, edited by A. Copping and L. Hemery, Ocean Energy Systems (OES), pp. 67–85

Guido, J. T. (2014) 'An Approach to the Active Defense of Wireless Radio Networks', *Doctoral dissertation, University of Colorado Colorado Springs*. Available at: http://www.jeffreyguido.com/work/tdoa_page.html.

Harrison, T. W., Clemett, N., Polagye, B., & Thomson, J. (2023) 'Experimental Validation of Float Array Tidal Current Measurements in Agate Pass, WA', *Journal of Atmospheric and Oceanic Technology*. Available at https://doi.org/10.1175/JTECH-D-22-0034.1.

Martin, S.B. *et al.* (2021a) 'Erratum: Hybrid millidecade spectra: A practical format for exchange of long-term ambient sound data [JASA Express Lett. **1** (1), 011203 (2021)]', *JASA Express Letters*, 1(8), p. 081201. Available at: https://doi.org/10.1121/10.0005818.

Martin, S.B. *et al.* (2021b) 'Hybrid millidecade spectra: A practical format for exchange of long-term ambient sound data', *JASA Express Letters*, 1(1), p. 011203. Available at: https://doi.org/10.1121/10.0003324.

Sayed, A.H., Tarighat, A. and Khajehnouri, N. (2005) 'Network-based wireless location: challenges faced in developing techniques for accurate wireless location information', *IEEE Signal Processing Magazine*, 22(4), pp. 24–40. Available at: https://doi.org/10.1109/MSP.2005.1458275.